Строительство уникальных зданий и сооружений. ISSN 2304-6295. 9 (60). 2017. 7-21

Construction of Unique Buildings and Structures

journal homepage: www.unistroy.spbstu.ru

GPR tomography as applied to delineation of voids

M.S. Sudakova [1], A.U. Kalashnikov [2], E.B. Terentieva [3*]

[1-3]*Lomonosov Moscow State University, GSP-1, Leninskie Gory, Moscow, 119991, Russia*

Article info

scientific article

doi: 10.18720/CUBS.60.1

Article history

Received: 09.11.2016

Keywords

Non-destructive testing;
electromagnetic methods;
forward and inverse problem solving;
mathematical modeling;
ground penetrating radar;
tomography;

ABSTRACT

This work presents the evaluation effectiveness of the GPR tomography for characterization of square voids in engineering structures. One of the columns of the iconic main building of the Moscow State University was selected as a target object with known configuration. Given that the heterogeneity of the column complicates the interpretation of GPR data acquired in reflection mode, transmission tomographic ray coverage was employed. Mathematical modelling and tomographic inversion to locate real objects were carried out. The radar tomography and the common-offset GPR geometry techniques are compared with respect to the acquired information about location, shape and dimensions of the void inside the column. The tomography results are characterized by high precision and are more reliable compared to the results of single-fold GPR survey.

Content

Contact information:

1 +7(495)93912307, m.s.sudakova@yandex.ru (Maria Sudakova, Ph.D., Senior Research Officer)
2 +7(495)9391230, x_kalash@mail.ru (Alexey Kalashnikov, Research Assistant)
3 * +7(926)7352288, genia_teren@mail.ru (Evgeniya Terentieva,Ph.D., Senior Lecturer)

1. Introduction

The non-destructive testing is a major and, in most cases, the only possible method of structure condition assessment. Commonly tested constructions are columns, building footings and bridges. The load-bearing capacity of constructions apart from concrete strength depends on defects of the internal structure: fractures, foreign inclusions and voids. Voids differ in size and origin. They may be required by design (air ducts, etc.) or developed in the course of construction damage.

The Ground Penetrating Radar (GPR) is one of the non-destructive methods commonly used for assessment of structures and buildings. This method has higher resolution compared to acoustic methods and it allows delineating internal structure and detecting anomalous zones, related to wet condition and cleavage. The most popular operation mode of GPR is the single-fold antenna geometry. It is the most cost-efficient, the least labour consuming and, consequently, the most commonly used method. GPR surveys in civil engineering are aimed at structural information acquisition: estimation of slabs thickness [1,2], detection and location of steel rebar or pipe hidden beneath the surface, estimation of integrity of metal elements [3], delineation of boundaries within the structure [1, 2, 4]. There are several examples demonstrating ability of the GPR technique to estimate material properties such as moisture or chloride content of concrete [5, 6, 7], location of large voids [8]. However, there have been reported difficulties in differentiation of air-filled void from other types of inhomogeneity within the section: rebars, boundaries of bricks etc. [9, 3, 4]. Based on these previous studies, the interpretation result is in most cases ambiguous and the information regarding the internal structure properties is qualitative.

Use of GPR tomography can address the above-mentioned disadvantages of the single-fold GPR operation mode. The tomographic ray coverage yields quantitative result: the acquired electromagnetic (EM) wave velocity and amplitude allows not only delineation of «anomalous zones», but also estimation of the moisture content of a structure as well as the volume of voids [10]. The application of direct signal with increased number of the observation points is more meaningful, as it enables acquisition of quantitative EM properties at every point of the studied volume. The technique complexity is leveraged by the quantity of the acquired information.

This paper presents the analysis of the GPR tomography potential during the detection of air-filled voids of various sizes by the example of isometric engineering structure. Mathematical modelling and field measurements were carried out for the case of a column with a known structure containing a void.

GPR tomography is similar to seismic tomography, as applied to EM field. The problem of recovering velocity in case of EM waves passing through a specified medium volume using known arrival times and transmitter and receiver positions has the same solution as in seismic tomography. During the last 20 years, seismic tomography has been widely applied to complex geological problems. A comprehensive review of the method is given in numerous papers [11]. Aki and Lee were the pioneers of seismic tomography. Their first tomography paper considered the problem of the earth crust velocity estimation in California area, with an earthquake being the seismic energy source [12]. Since that time, the method has undergone many innovations by means of improvement of forward and inverse problem solutions, processed data volume growth and hardware development. The existing algorithms of tomographic inversion produce good imaging results for most of the geophysical models. However, a few problems are considered to be complicated for implementation and subsequent analysis.

One of these is a problem of detection and delineation of areas characterized by considerable positive or negative velocity contrast with the host medium. The difficulties arise in estimation of the anomaly size as well as in its delineation. The velocity anomaly leads to the following phenomenon: the velocity contrast between the rocks is distributed through the whole medium, and the boundary between the blocks of the medium becomes vague [10]. In a number of papers [13] the authors report successful use of the so-called “irregular” algorithm of 3D travel-time tomography ray tracing. The “irregular” ray-tracing approach allows suppressing artefacts caused by noise and high velocity contrast and considerably improving the solution given noisy or inconsistent travel-time data even for high velocity contrast anomalies (more than 20%) in the target region. Earlier this approach was demonstrated for the 2D case [14, 15, 16].

Mathematical and physical modelling is often helpful to researchers. For instance, an approach for 3D travel-time tomography, which works well in reconstructing high contrast velocity anomalies in the case of cross-well observation geometry is analysed in [17]. Based on results of physical and numerical modelling the authors demonstrated, that «when the velocity contrast is greater than 30%, the tomographic result will be deformed significantly, when it is between 30% and 15%, it will be acceptable, and when it is less than 15%, it will be very good» [17]. The authors attribute this effect to irregular ray coverage and insufficient grid sampling; however, they use more than 100 source points and the same number of receiver points in modelling, considering the anomaly size of about 50% of the model area.

The same mathematical algorithms accomplish tomographic inversion of GPR data, as in seismic exploration. That is why all of the above-mentioned conclusions are applicable to GPR tomography.

The velocity of EM wave in the air is 30 cm/ns, while in concrete it is about 10-12 cm/ns, i.e. the observed velocity contrast for the case of an air chamber is far more than 30%, which is typical for seismic exploration.

Application of the GPR tomography [18, 19, 20] is widespread to name just a few. Most of papers deal with the crosshole radar tomography used for high-resolution characterization of the shallow subsurface between boreholes. For instance, the problem of local high velocity anomaly (15% contrast) reconstruction using crosshole radar tomography is solved [19]. The problem of location and quantification of voids and of larger deteriorated areas in masonry structures using radar tomography was addressed in paper [20]. The authors succeeded in recovering the size of voids with adequate accuracy. Yet as opposed to the size of voids, the velocity value in air-filled void was recovered with a 30% departure from the accepted reference value. Therefore, the problem of high contrast anomaly recovery (more than 30% contrast as in our case) using radar tomography potential appears to be attractive and up-to-date. This problem can be solved using mathematical and physical modelling, as well as field measurements on the objects with known structure.

2. Methods

The data type used in tomographic inversion imposes its division into ray, diffraction and full-waveform modifications. The wavelengths used in ray tomography are much smaller than the size of inhomogeneities under study. On the other hand, the long-wavelength approach is used in diffraction tomography. Currently the methods of ray tomography are most commonly used for study of three-dimensional velocity inhomogeneities. Ray tomography involves representation of input data in a form of composite functions along the lines (rays) in space. Ray theory approach presumes energy propagation along ray tubes of finite thickness, as a function of a wavelength. For this reason, a large number of rays results in complete coverage of the study area by a beam tube [21].

2.1. Ray tomography

One of the fundamental equations of ray tomography is the eikonal equation, which relates the arrival time of the wave to a specified point to the corresponding velocity distribution. The eikonal equation (1) in two dimensions (corresponding to the scalar wave equation) can be written:

$$(\frac{\partial t}{\partial x})^2 + (\frac{\partial t}{\partial z})^2 = s(x,z)^2 \quad (1)$$

Where $s = \frac{1}{V(r)}$ is the parameter, inverse to velocity and called *slowness*. The components of *s* must be mutually orthogonal. The traveltime function - *t*, is constant along a wavefront surface. Equation (1) is an expression for the magnitude of the slowness vector. This equation is the basic equation of ray tomography; it allows calculating time fields and ray paths of seismic waves.

The equation (1) implies the following corollary – an integral that expresses the wave traveltime along a ray path P from the i^{th} source point to the j^{th} receiver point (2):

$$T_{ij} = \int_{P_{ij}} \frac{dl}{V(r)} = \int_{P_{ij}} s dl \quad (2)$$

The inverse problem solution is based on the search of *V(r)* from the given T_{ij} distributions. In the high-frequency approximation, the traveltime function is governed by the eikonal equation [22].

Since the ray path is a function of velocity, the function of arrival time is nonlinear. The Fermat Principle is applied for linearization. The details of the tomography problem solution can be found, for example, in the paper [11].

Assume that the travel time for the starting (or so-called background) model is equal to T_0 (3):

$$T_0 = \int_{P_0} \frac{dl}{V_0(r)} \quad (3)$$

We can derive the integral along the whole path P_0, calculated for the background model. This approach facilitates ray tracing by choosing a layered background model to calculate the path P_0 (4):

$$T \cong \int_{P_0} \frac{dl}{V(r)} \quad (4)$$

Subtraction gives a linearized relationship (5) that expresses the traveltime delay δT:

$$\delta T = T - T_0 \approx \int_{P_0} (\frac{1}{V} - \frac{1}{V_0}) dl \approx -\int_{P_0} \frac{\delta V(r)}{V^2} dl \quad (5)$$

Where $\delta V(r)$ – being the velocity anomaly of a model.

As a result, we derive an approximate linear relationship between $\delta V(r)$ and deviation between the time values T and T_0 on assumption that the ray path remains unchanged. The problem is reduced to finding $\delta V(r)$ from the known time deviation.

Several assumptions are made when performing ray-based tomography: the validity of ray-theory (the "infinite" frequency assumption) and linearity of the inverse problem. If the anomalies perturbing the ray paths have large contrasts with the physical properties of the host medium and have sizes of approximately the same order as the wavelength, the basic assumptions of the ray tomography break down. Consequently, the estimated traveltime delay measurements have systematic errors. These errors are attributed to so-called wave front healing – the interference of directly travelling waves with the waves diffracted around anomalies [23; 24].

2.2. Study object

One of the columns of the main building of Moscow State University (MSU) was selected as a target object with known configuration. According to the data provided by the engineering service of the MSU, the column has the structure, presented in Figure 1 The column's horizontal section is a square of side 1.5m, with a square void in the center, measuring 70cm by 70cm. The column is encased in granite. There are several concrete layers under the granite coating. The thickness of the granite-concrete layer is 40cm on each side.

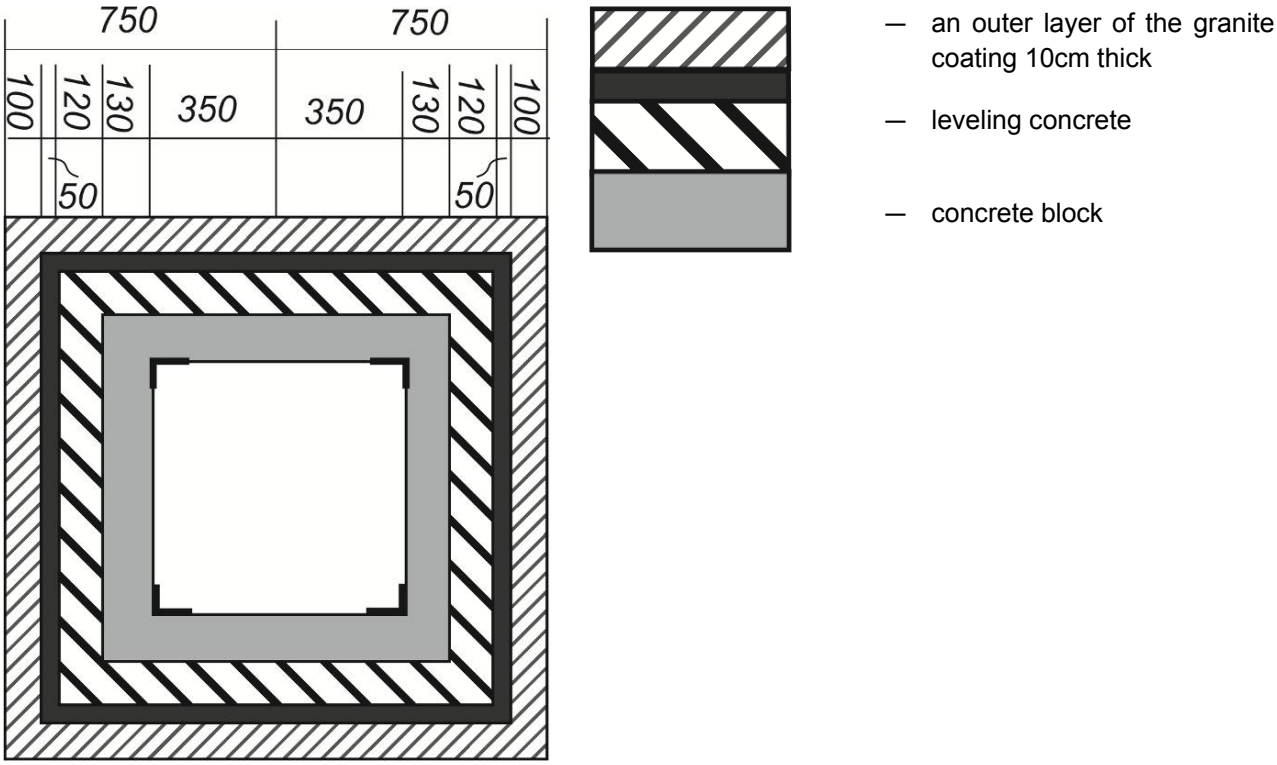

Figure 1. Design-basis column configuration. Section in a horizontal plane. The figures correspond to the thickness of layers and the size of a void (white filling) in mm.

2.3. GPR survey using single-fold GPR antenna geometry

First, the GPR survey on the column was performed using single-fold GPR antenna geometry. A georadar Zond 12e (RadarSystems Riga, Latvia EU) with a 2000 MHz center frequency antenna was used for a single fold survey. The antenna was pulled directly over the surface, with the tie performed with a survey-wheel odometer. During the radar acquisition the record length was 50 ns, the sampling rate was 0.01 ns.

2.4. Mathematical modelling

In order to study tomography potential and to select the parameters of field measurements, we have executed mathematical modelling. The model represents an engineering construction with dimensions comparable to the actual one.

The wavelength in real medium is likely to be of the order of 10cm when using the 2GHz antenna. Therefore, the void size was set to vary from 10cm (about 1 wavelength, at the boundary of the method resolution) to 70cm (half the linear size of the entire model, about several wavelengths) in our modelling.

Three configurations of void position have been tested for modelling: in the corner of the model, in the center of the model and against the wall. The modeled size and position variations describe most possible cases, given a unit void inside a concrete structure. **Ошибка! Источник ссылки не найден.**a features a schematic representation one of a simulated media (model 2, void in center).

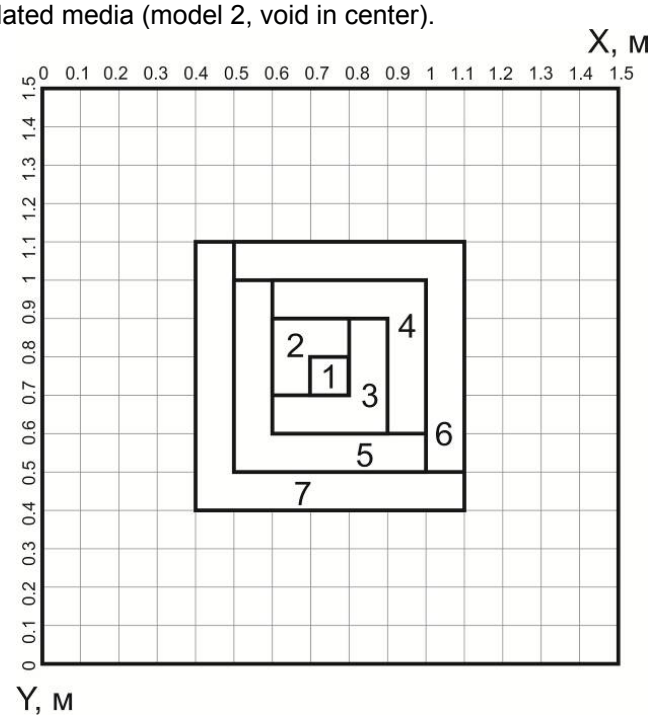

Figure 2. Assessed Model 2 of engineering structure containing a void (the void is in the center of a model). The figures designate the model numbers and the void sizes in decimeters. The grid cells are indicated by fine gray line.

The radiation and receiver points were situated on the two opposite faces of the square model with transmitter and receiver intervals equal to 10 cm. 14X14 array of receivers and transmitters for the two opposite faces make 392 data sets (Figure 3). The transmitter points are marked by «S», while the receivers by «R».

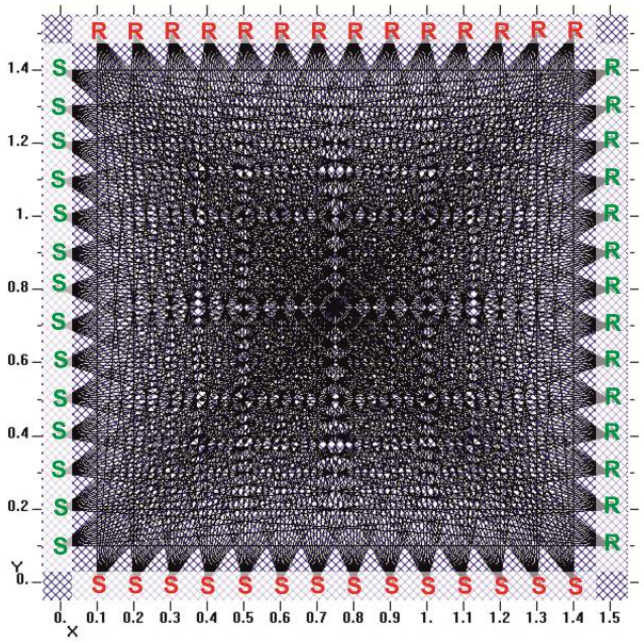

Figure 3. Raypaths and positions of transmitters and receivers. The transmitters are marked by «S», while the receivers - by «R».

The calculations were carried out using the software “GeoTomCG” (GeoTom, LLC) by Daryl Tweeton. The main principles and the computing algorithm are laid down in [26]. The software involves calculation on a regular mesh with rectangular cells. GeoTomCG performs inversions with simultaneous iterative reconstruction technique, or SIRT and allows straight and curved ray tracing [27, 28, 29]. Curved ray tracing in GeoTomCG is performed with a revised form of ray bending, derived from the Um and Thurber method with modifications yielding more reliable results [30].

The first stage involved calculation of travel time for the given void-containing model (forward problem solving). The first break times were calculated for each model (see **Ошибка! Источник ссылки не найден.**) with corresponding acquisition geometry (Figure 3). The second stage involved solving the inverse problem using the calculated time values. The initial model was characterized by two constant-velocity approximations: V=12cm/ns - velocity in void-free structure and V=Vrms, where Vrms – is the root-mean-square velocity throughout the arrival times with the assumption of direct rays. The root-mean-square velocity increased from 12.4cm/ns in the presence of a void with dimensions of 10x10 cm to 13.4cm/ns for the void with dimensions of 70x70cm. Although this variation lied within the limits of 12% of the model velocity, the velocity increase would implicitly indicate the occurrence of a void in case of noise-free data. The number of iterations for each inverse problem was equal to 40; the problem was solved for curved rays. The cell size was 10x10 cm. The iterative process was tailored in such a way that the iteration index increase provoked the decrease of the mean-square and the total deviation values.

The analysis of the errors showed that the increase of void dimensions from 10x10 cm to 70x70 cm leads to the increase of deviation by two orders of magnitude: from 0.0025ns for the minimal void, to 0.5ns for the maximum void located in a corner. The calculation error was also affected by the void position: the minimum mean-square deviation corresponded to the corner void position, while the maximum – to the void position against the wall.

2.5. GPR tomographic measurements on the known construction

GPR tomographic measurements of the column with known construction presented in Figure 1, were carried out in order to test the calculations.

The radar Zond 12e manufactured by RadarSystems (Riga, Latvia EU) with 2000 MHz antenna was used for tomography studies. The transmitter was moved along the labelled points in discrete mode. (Figure 4.) The receiver was moved along the labelled points in discrete mode, while transmitter was held at the same position. After changing the transmitter position, the receiver antenna was moved from point to point. The record length was 50 ns and the sampling rate was 0.01 ns. The acquisition was executed without stacking and filtering. The traveltime calibration is carried out by measuring the so-called “air pulse” (from transmitter antenna to receiver antenna).

Figure 4. Field measurement on a column demonstrating the studied object and the equipment.

Consequently, we performed first break picks for all radargrams. Figure 5 presents one of the radargrams and an example of the first break picks. The red line represents calculated time values for the model 2 (void in the center), the void size of 70 cm, and the transmitter position at 0.6m. The mismatch of arrival times can be a result of inhomogeneous column structure.

The starting model parameter used for the calculation of the inverse tomographic transform was Vrms=12cm/ns. The calculation involved curved rays; the mean-square mis-tie was 0.08 ns, while the total mis-tie was about 1.3 ns.

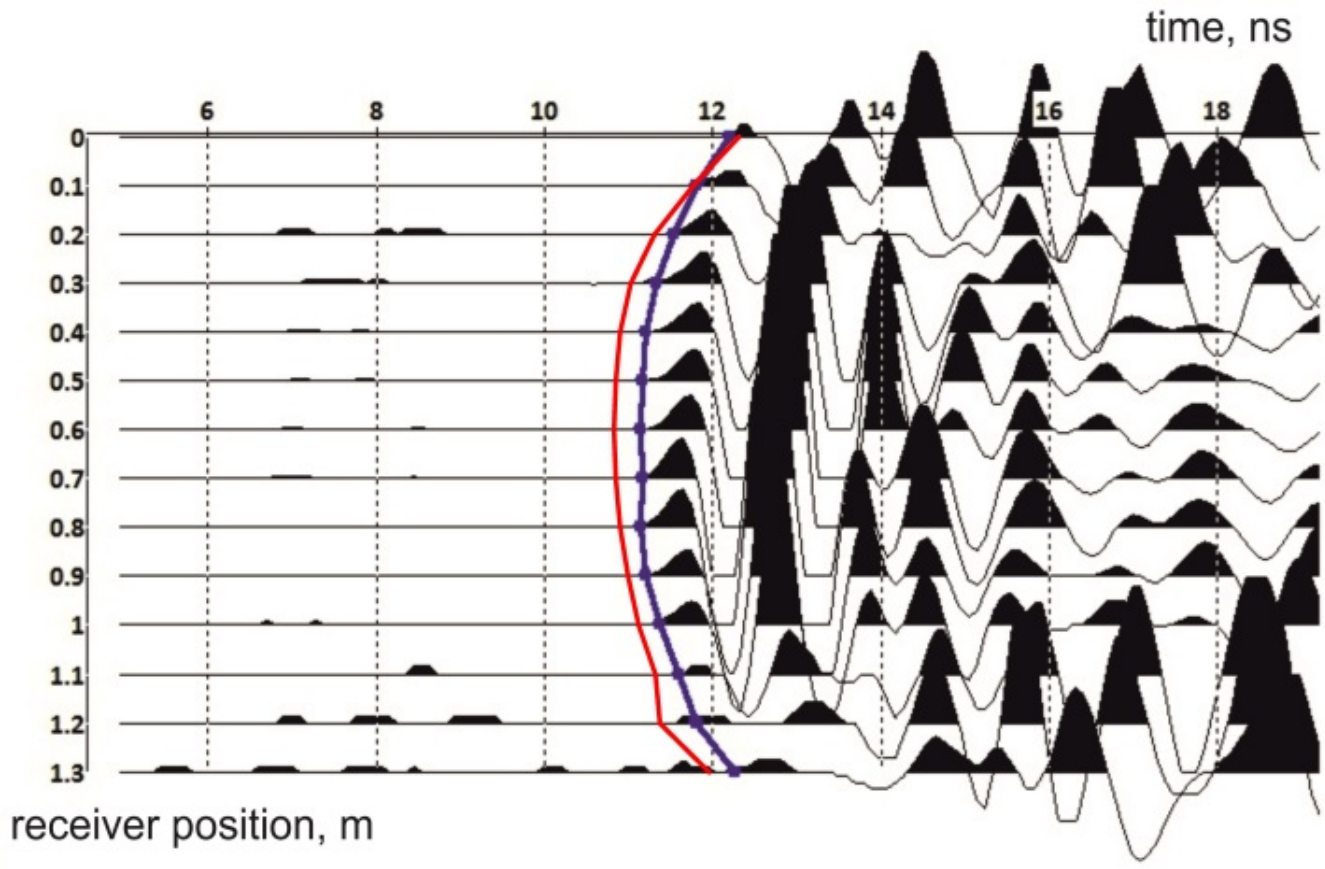

Figure 5. Example of GPR tomography data (the transmitter antenna position is at 0.6m) with an example of first break picks (the blue line). The time delay is 2ns. The red line designates the calculated time values for the model 2 (the void in the center), the void size is 70 cm; the transmitter position is at 0.6m. The mismatch of arrival times can be attributed to inhomogeneous column structure.

3. Results and discussion

3.1. GPR survey on using single-fold GPR antenna geometry

The radargram, acquired using single-fold antenna geometry is presented in Figure 6. The measurements were executed on each side of the column, the interval between the vertical markers corresponds to each side in Figure 6. An example of line drawing corresponding to possible boundaries is presented in Figure 7. The radargram demonstrates coherent events; however its interpretation significantly differs from the design-basis column configuration : neither amplitude variation, no multiple reflections that might be indicative of a void are observed. As is argued in [25] the estimation of void size using single-fold antenna geometry is unfeasible. Both figures (Figure 6 and Figure 7) demonstrate a complex pattern of the wavefield, which consequently implies non-unique interpretation.

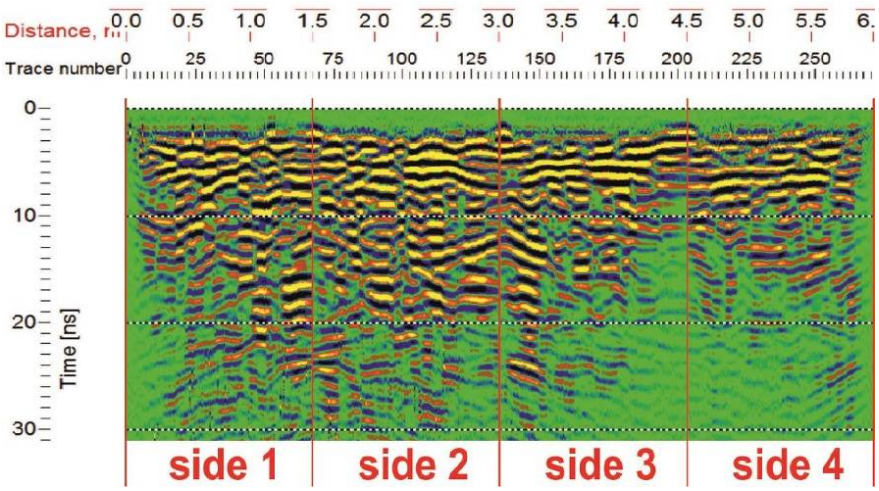

Figure 6. Radargram, acquired on the column presented in Fig.1 using single-fold antenna geometry.

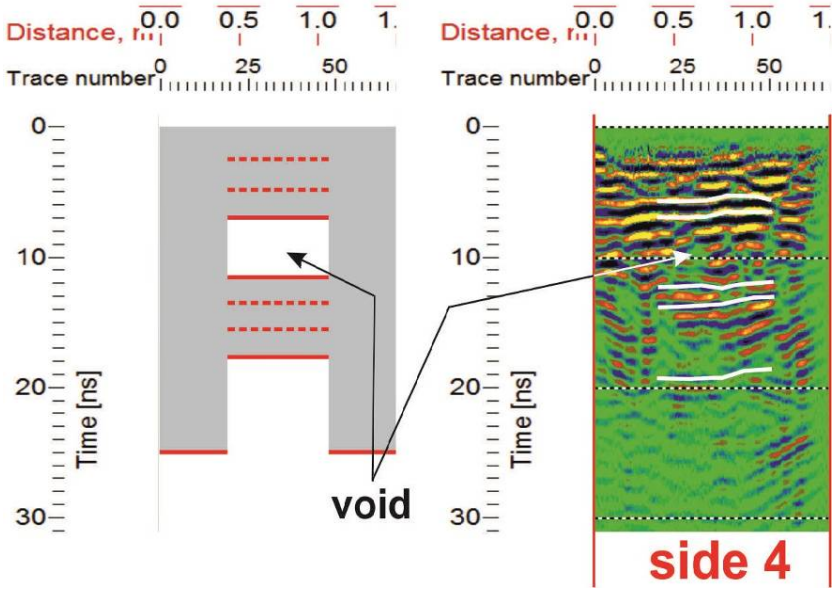

Figure 7. Interpretation (A) and the corresponding radargram (B) acquired on one of the sides of the column in single fold geometry. The white line drawing corresponding to possible boundaries.

3.2. Mathematical Modelling

Figure 8a presents results of mathematical modelling: calculated velocity distribution (derived for the sizes of voids 10cm, 20cm, 40cm and 70cm) and different starting velocities for model 2 (void in center). The black box indicates the void position.

Figure 8b shows ray paths, for the void sized 40cm. The theoretic ray paths for the forward problem (the second column from the left) differ from those calculated for the inverse problem (two columns on the right); however, one can see a refraction on the anomaly boundary. There are no principal differences among ray paths for different starting velocity approximations.

The results show:

The voids with dimensions exceeding 20cm are delineated with higher confidence, regardless of their position (Figure 8a). The void is not clearly distinguishable on velocity sections if the void size is less than 10 cm. The latter may be caused by under-sampling of measurement grid.

The indicators of voids: more than 30% velocity increase (for the void size of 20 cm), and more than 100% velocity increase (for the void size of 70 cm); ray bending at the boundary of the high-velocity area, coinciding with a theoretical void boundary (Figure 8b).

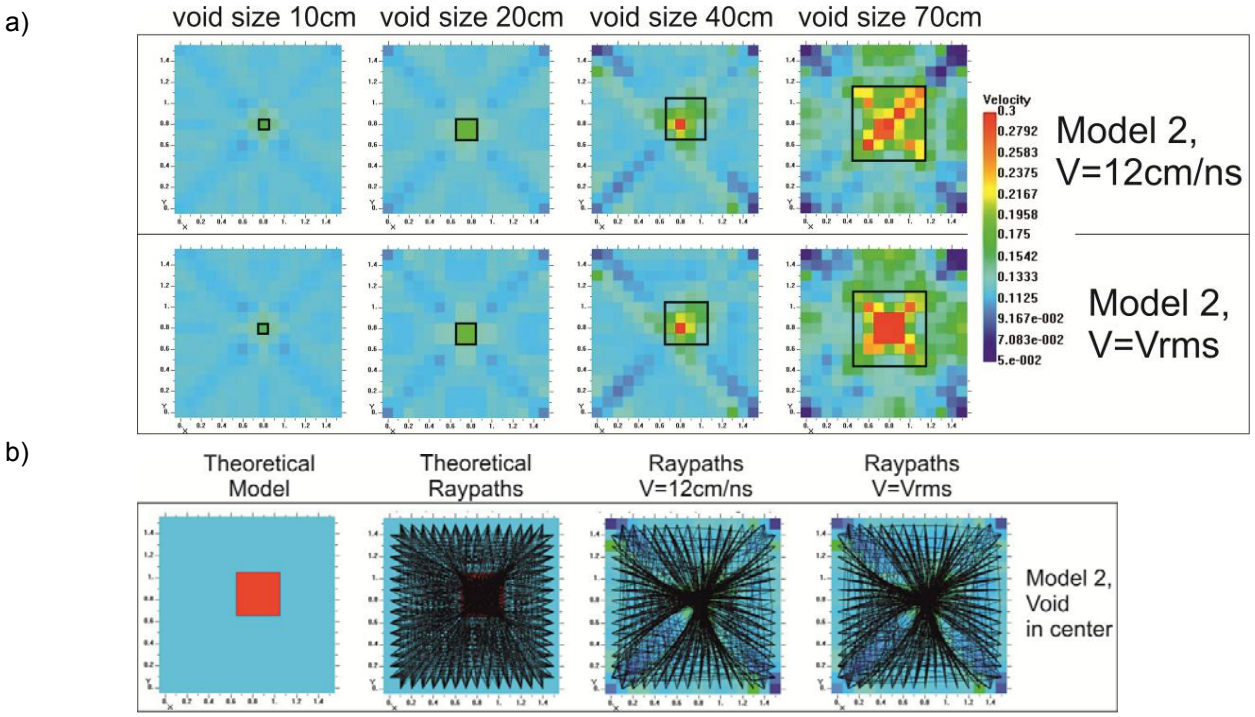

Figure 8. a) Some results of mathematical modelling (the inverse problem). The black frame indicates the assigned void position. The velocity is given in m/ns b) Theoretical (forward problem) and calculated ray paths (inverse problem) for model with void size 40cm. The axes labels are in meters.

3.3. GPR tomographic measurements on the known construction

Figure 9 illustrates the result of tomographic inversion of times measured on the column (a), and the ray paths for the given velocity distribution (b). The specified void is marked by a black box.

Figure 9 demonstrates that velocity values vary from 10 to 30 cm/ns. A zone of higher velocity in the radar tomogram was observed in the center of the velocity section, which fits to the location of the void (the black box indicates the area with velocity range of 25-30 cm/ns, corresponding to velocity value in the air).

The problem of air-filled void delineation is solved: the tomogram in Figure 9 shows a clear and sharp separation of the anomaly.

A modelling-prompted air-filled void indicator, i.e. ray bending phenomenon was observed at the boundary of a void (Figure 9b). Moreover, velocity values inside a void exceeded velocity values in solid part by more than 30%. However, the average velocity in solid part was 17cm/ns. Based on results of the mathematical modelling, we can conclude, that the given velocity value was higher than the normal velocity for concrete. This artefact can be attributed to the poor algorithm performance. Most of researchers state, that ray-bending algorithms can sometimes lead to unreliable resolution, especially at interfaces of abrupt dielectric changes.

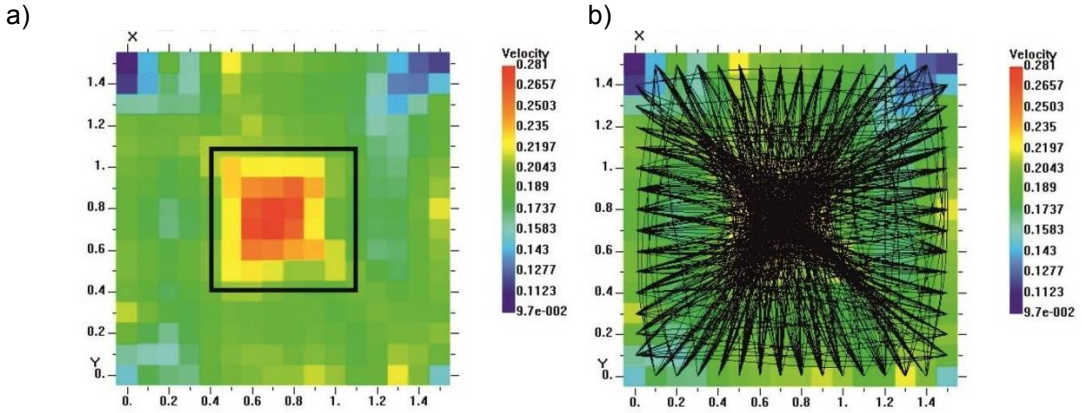

Figure 9. Practical problem solving: a) inversion result, b) superposition of inversion result and ray coverage. Velocity is given in m/ns. The axes labels are in meters.

The next stage of tomographic inversion included calculations with a more complex initial model: the initial model with known void in the center of the column (see Fig.1 – column configuration). The result of tomographic inversion based on the initial model is demonstrated in Figure 10. Given the initial model with known air-filled void, the layered structure of the column can be seen (compare Fig.1 and Figure 10). This kind of quality can only be achieved with a lot of previous data checks, an adapted starting model as it is published in [19] and [31].Similarly, this is the case of small-size high-velocity anomaly, related to real crack observed on the surface of the column (Figure 10). We observe the velocity anomaly obviously corresponding to the crack; however, the data available do not allow estimating the size of the crack (especially its 3D structure under the granite coating).

It is worth pointing out that common offset radargrams resulted in complicated images, which was also observed by [3] and it was not possible to differentiate between reflections on cracks and reflections on pieces of granite coating, and the final radargrams result in complicated images. Consequently, a comparison between the method based on the common offset acquisition and the tomographic technique shows that more sophisticated tomographic acquisition technique results in quantitative consistent results. Limitations in the resolution achievable by tomographic inversion are partly limited by the number of artefacts, which appeared in the results. Accuracy in reconstructing velocity images is controlled by density coverage of raypaths in the tomographic sections. One of possible solutions to account for problem from the ray-based inversion is the full waveform inversion [31]. However, the full waveform inversion comes at a cost of huge computing time and the computer resolving power needed [32].

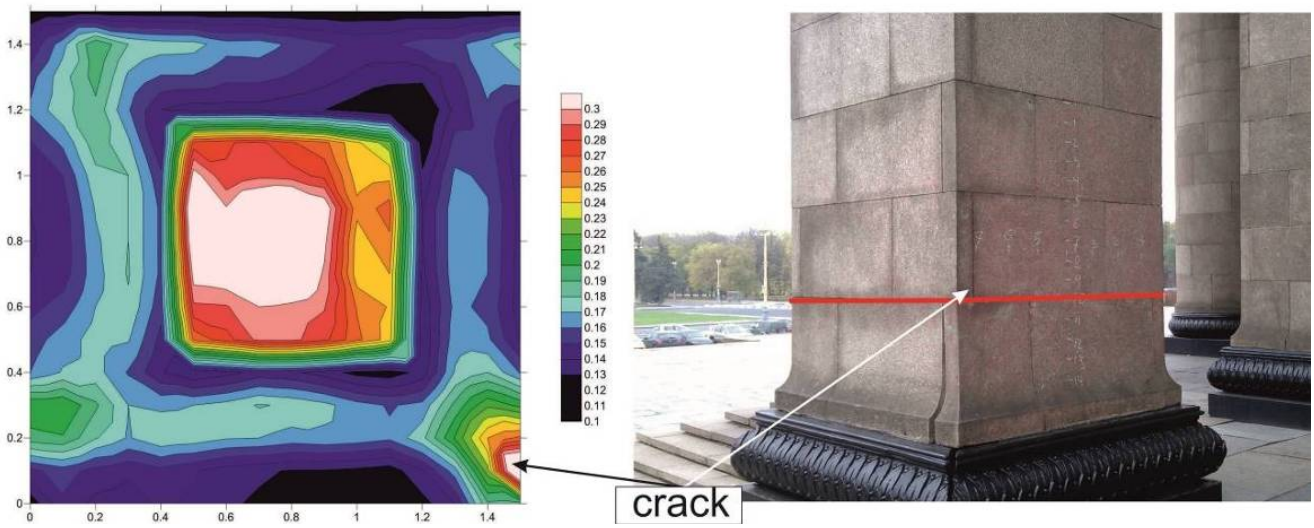

Figure 10. Result of tomography with initial model with known void in the center. Constant velocity contours presentation (left) and section plane position on a column (right, red line). Velocity is given in m/ns. The axes labels are in meters. The white arrow designates the granite coating gap, which corresponds to the high-velocity anomaly on the velocity section.

4. Conclusion

The mathematical modelling and field measurements demonstrated that:

1. GPR tomography is a reasonable solution for the problem of voids detection inside engineering structures. Despite of the upfront labour input, the acquired results are characterized by high quality and are more reliable compared to the results of single-fold GPR survey.

2. The voids measuring more than 20 cm can be successfully delineated, regardless of their position, based on the following indicators: ray bending at the boundary of the void and velocity increase by more than 30%.

3. The mathematic modelling has demonstrated that GPR tomography may be suboptimal for void delineation, when the void measures less than 10 cm, given the transmitter and receiver offset equals to 10 cm.

4. Simultaneous estimation of EM velocity distribution in a solid part of the column and correct velocity estimation inside a void is problematic due to inaccuracy.

5. Increase of the number of parameters of the known objects under study can improve the model tuning, which in turn could significantly enhance the stability and reliability of problem solution. Owing to these improvements, higher precision of anomaly detection and better size estimation can be achieved.

The advanced tomographic technique will be extensively used by construction companies, structure and infrastructures owners who seek accurate geometrical information through using cost-effective solutions. However, there is still a need to adapt software tomography algorithms and signal processing techniques.

References

[1] Barrile V. and R. Pucinotti. Application of radar technology to reinforced concrete structures: A case study. NDT & E International, 2005. Vol. 38 (7). pp. 596–604.

[2] Hugenschmidt J. Concrete bridge inspection with a mobile GPR system. Construction and Building Materials. 2002. Vol. 16. pp. 147 – 154.

[3] Santos-Assunçao S., Perez-Gracia V., Caselles O., Clapes J. and Salinas V. Assessment of Complex Masonry Structures with GPR Compared to Other Non-Destructive Testing Studies. Remote Sensing. 2014. Vol. 6. Pp. 8220-8237; doi: 10.3390/rs6098220.

[4] Hamrouche R., Klysz G., Balayssac J.-P., Rhazi J. and Ballivy G. Numerical Simulations and Laboratory Tests to Explore the Potential of Ground-Penetrating Radar (GPR) in Detecting Unfilled Joints in Brick Masonry Structures. International Journal of Architectural Heritage: Conservation, Analysis, and Restoration. 2012. 6:6. Pp. 648-664.

[5] Sbartaï Z. M., Laurens S., Balayssac J.-P., Arliguie G. and Ballivy G. Ability of the direct wave of radar ground-coupled antenna for NDT of concrete structures. NDT & E International. 2006. Vol. 39 (5). Pp. 400–407.

[6] Klysz G., and J.-P Balayssac. Determination of volumetric water content of concrete using ground–penetrating radar. Cement and Concrete Research. 2007. Vol. 37(8). Pp. 1164–1171.

[7] Hugenschmidt J., Loser R. Detection of chlorides and moisture in concrete structures with Ground penetrating radar. Materials and Structures. 2008. Vol. 41. Pp. 785-792.

[8] Maierhofer C., and Leipold S. Radar investigation of masonry structures. NDT & E International. 2001. Vol. 34 (2). Pp. 139–147.

[9] Roberts R., Corcoran K., Arvanitis M., and Schutz A. Insulated Concrete form Void Detection Using Ground Penetrating Radar. In: PIERS Proceedings, 2011. Marrakesh, MOROCCO, March 20-23.

[10] Mathewson J. C., Evans D., Leone C., Leathard M., Dangerfield J., Tonning S. A. Improved imaging and resolution of overburden heterogeneity by combining amplitude inversion and tomography. 2012. SEG 2012 Annual Meeting. 5. Las Vegas. Pp. 4271-4274.

[11] Nolet G. A breviary of seismic tomography, imaging the Interior of the Earth and Sun. 2008. Cambridge: Cambridge University Press.

[12] Aki K., Lee W.H.K. Determination of the three-dimensional velocity anomalies under a seismic array using first P arrival times from local earthquakes. 1976. 1. A homogeneous intial model. Journal of Geophysical Research. Vol. 81. pp. 4381–4399.

[13] Chao-Ying Bai and Stewart Greenhalgh. 3-D Non-linear Travel-time Tomography: Imaging High Contrast. Pure and Applied Geophysics. 2005. Vol. 162. pp. 2029–2049.

[14] Moser T. J. Shortest Path Calculation of Seismic Rays. Geophysics. 1991. Vol. 56. pp. 59–67.

[15] Gruber T. and Greenhalgh S.A. Short Note: Precision Analysis of First-break times in Grid Models. Geophysics. 1998. vol. 63. pp. 1062–1065.

[16] Fischer R. and Lees J.M. Shortest Path Ray Tracing with Sparse Graphs. Geophysics. 1994. vol. 58. pp. 987–996.

[17] Chen Guo-Jin, Cao Hui, Wu Tong-Shuan, Zou Fei, Yao Zhen-Zing. Effects of velocity contrast on the quality of crosswell traveltime tomography and an imploved method. Chinese Journal of geophysics. 2006. vol. 49 (3). pp. 810-818.

[18] Hauser, K., Jackson, M., Lane, J., Hodges, R. Deep tunnel detection using crosshole radar tomography. Proceedings SAGEEP'95. 1995. Orlando, FL. pp. 853–857.

[19] Tronicke J., Tweeton, D.R., Dietrich P., Appel E. Improved crosshole radar tomography by using direct and reflected arrival times. Journal of Applied Geophysics. 2001. Vol. 47. pp. 97–105.

[20] Wenfrich A., Trela Ch., Krause M., Maierhofer Ch., Effner U., Wostmann J. Location of Voids in Masonry Structures by Using Radar and Ultrasonic Traveltime Tomography. In: Tu.3.2.5 Bundesanstalt für Materialforschung und –prüfung (BAM). Berlin: ECNDT Tu.3.2.5 Bundesanstalt für Materialforschung und –prüfung (BAM). 2006. Berlin. Germany.

[21] YAnovskaya T.B. Problemy sejsmotomografii // Problemy geotomografii. M.: Nauka, 1997. S. 86-98.Bleistein N. Mathematical methods for wave phenomena. Academic Press, 1984. p. 341.

[22] Hung, S., Dahlen, F. & Nolet, G. Wavefront healing: a banana-doughnut perspective. Geophys. J. Int. 2001. vol. 146. pp. 289–312.

[23] Malcolm A.E., Trampert J., Tomographic errors from wave front healing: more than just a fast bias. Geophys. J. Int. 2011. Vol. 185 (1). pp. 385–402.

[24] Starovoytov A.V., Romanova A.M., Kalashnikov A.Yu. GPR study of depressed areas in the upper cross-section. EAGE Near Surface. 2011. Manchester, UK.

[25] Tweeton, D.R., Jackson M.J. and K.S. Roessler. BOMCRATR – A Curved Ray Tomographic Computer Program for Geophysical Applications. 1992. USBM RI 9411. 39.

[26] Lytle R.J, Dines K.A., Laine E.F., and Lager D.L. Electromagnetic Cross-Borehole Survey of a Site Proposed for an Urban Transit Station.1978. UCRL-52484, Lawrence Livermore Laboratory. University of California. 19.

[27] Peterson J. E., Paulson B. N. P., and McEvilly T. V. Applications of Algebraic Reconstruction Techniques to Crosshole Seismic Data. Geophysics. 1985. Vol. 50. pp. 1566-1580.

[28] Lehmann B. Seismic Traveltime Tomography for Engineering and Exploration Applications. 2007. EAGE Publications bv, DB Houton, the Netherlands. pp. 28-32.

[29] Um, J. and C. Thurber. A Fast Algorithm for Two-Point Seismic Ray Tracing. Bulletin of Seismological Society of America. 1987. Vol. 77. pp. 972-986.

[30] Ernst J., Green A., Maurer H., and Holliger K. Application of a new 2D time-domain full-waveform inversion scheme to crosshole radar data. GEOPHYSICS, September-October 2007, Vol. 72. No. 5 : pp. J53-J64

[31] Watson. F. Towards 3D full-wave inversion for GPR. 2016 IEEE Radar Conference (RadarConf). 1-6.

Георадарная томография применительно к выявлению пустот

М.С. Судакова[1], А.Ю. Калашников[2], Е.Б. Терентьева [3*]

[1-3]Московский государственный университет им. М. В. Ломоносова,119991, Россия, Москва, ГСП-1, ул. Ленинские Горы, д.1

ИНФОРМАЦИЯ О СТАТЬЕ	ИСТОРИЯ	КЛЮЧЕВЫЕ СЛОВА
doi: 10.18720/CUBS.60.1	Подана в редакцию: 09.11.2016	неразрушающий контроль; электромагнитные методы; решения прямой и обратной задачи; математическое моделирование; георадар; томография;

АННОТАЦИЯ

В работе представлена оценка эффективности георадарной томографии, направленной на поиск и описание квадратных пустот в инженерных структурах. Объектом исследования была одна из колонн главного здания МГУ с известной конструкцией. Неоднородность строения колонны сильно затрудняет интерпретацию данных георадарного профилирования и делает невозможным поиск пустоты, находящейся внутри колонны, поэтому нами была применена томографическая методика. Были выполнены математическое моделирование и томографическое обращение для оконтуривания пустоты. Нами выполнено сравнение результатов георадарной томографии и традиционного георадарного профилирования с точки зрения полученной информации о местоположении, форме и размерах пустоты внутри колонны. Результаты томографического обращения характеризуются более высокой точностью и достоверностью по сравнению с традиционной георадарной методикой.

Контакты авторов:

1 +7(495)9391230, m.s.sudakova@yandex.ru (Судакова Мария Сергеевна, к.т.н., научный сотрудник)
2 +7(495)9391230, x_kalash@mail.ru (Калашников Алексей Юрьевич, младший научный сотрудник)
3 * +7(926)7352288, genia_teren@mail.ru (Терентьева Евгения Борисовна, к.т.н., старший преподаватель)

Литература

[1] Barrile V., and R. Pucinotti. Application of radar technology to reinforced concrete structures: A case study. NDT & E International,2005. Vol. 38 (7). pp. 596–604.

[2] Hugenschmidt J. Concrete bridge inspection with a mobile GPR system. Construction and Building Materials. 2002. Vol. 16. pp. 147 – 154.

[3] Santos-Assunçao S., Perez-Gracia V., Caselles O., Clapes J. and Salinas V. Assessment of Complex Masonry Structures with GPR Compared to Other Non-Destructive Testing Studies. Remote Sensing. 2014. Vol. 6. pp. 8220-8237; doi:10.3390/rs6098220.

[4] Hamrouche R., Klysz G., Balayssac J.-P., Rhazi J. and Ballivy G. Numerical Simulations and Laboratory Tests to Explore the Potential of Ground-Penetrating Radar (GPR) in Detecting Unfilled Joints in Brick Masonry Structures. International Journal of Architectural Heritage: Conservation, Analysis, and Restoration. 2012. 6:6. pp. 648-664.

[5] Sbartaï Z. M., Laurens S., Balayssac J.-P., Arliguie G. and Ballivy G. Ability of the direct wave of radar ground-coupled antenna for NDT of concrete structures. NDT & E International. 2006. Vol. 39 (5). pp. 400–407.

[6] Klysz G., and J.-P Balayssac. Determination of volumetric water content of concrete using ground–penetrating radar. Cement and Concrete Research. 2007. Vol. 37(8). pp. 1164–1171.

[7] Hugenschmidt J., Loser R. Detection of chlorides and moisture in concrete structures with Ground penetrating radar. Materials and Structures. 2008. Vol. 41. pp. 785-792.

[8] Maierhofer C., and Leipold S. Radar investigation of masonry structures. NDT & E International. 2001. Vol. 34 (2). pp. 139–147.

[9] Roberts R., Corcoran K., Arvanitis M., and Schutz A. Insulated Concrete form Void Detection Using Ground Penetrating Radar. In: PIERS Proceedings, 2011. Marrakesh, MOROCCO, March 20-23.

[10] Mathewson J. C., Evans D., Leone C., Leathard M., Dangerfield J., Tonning S. A. Improved imaging and resolution of overburden heterogeneity by combining amplitude inversion and tomography. 2012. SEG 2012 Annual Meeting. 5. Las Vegas. Pp. 4271-4274.

[11] Nolet G. A breviary of seismic tomography, imaging the Interior of the Earth and Sun. 2008. Cambridge: Cambridge University Press.

[12] Aki K., Lee W.H.K. Determination of the three-dimensional velocity anomalies under a seismic array using first P arrival times from local earthquakes. 1976. 1. A homogeneous intial model. Journal of Geophysical Research. Vol. 81. pp. 4381–4399.

[13] Chao-Ying Bai and Stewart Greenhalgh. 3-D Non-linear Travel-time Tomography: Imaging High Contrast. Pure and Applied Geophysics. 2005. Vol. 162. pp. 2029–2049.

[14] Moser T. J. Shortest Path Calculation of Seismic Rays. Geophysics. 1991. Vol. 56. pp. 59–67.

[15] Gruber T. and Greenhalgh S.A. Short Note: Precision Analysis of First-break times in Grid Models. Geophysics. 1998. vol. 63. pp. 1062–1065.

[16] Fischer R. and Lees J.M. Shortest Path Ray Tracing with Sparse Graphs. Geophysics. 1994. vol. 58. pp. 987–996.

[17] Chen Guo-Jin, Cao Hui, Wu Tong-Shuan, Zou Fei, Yao Zhen-Zing. Effects of velocity contrast on the quality of crosswell traveltime tomography and an imploved method. Chinese Journal of geophysics. 2006. vol. 49 (3). pp. 810-818.

[18] Hauser, K., Jackson, M., Lane, J., Hodges, R. Deep tunnel detection using crosshole radar tomography. Proceedings SAGEEP'95. 1995. Orlando, FL. pp. 853–857.

[19] Tronicke J., Tweeton, D.R., Dietrich P., Appel E. Improved crosshole radar tomography by using direct and reflected arrival times. Journal of Applied Geophysics. 2001. Vol. 47. pp. 97–105.

[20] Wenfrich A., Trela Ch., Krause M., Maierhofer Ch., Effner U., Wostmann J. Location of Voids in Masonry Structures by Using Radar and Ultrasonic Traveltime Tomography. In: Tu.3.2.5 Bundesanstalt für Materialforschung und –prüfung (BAM). Berlin: ECNDT Tu.3.2.5 Bundesanstalt für Materialforschung und –prüfung (BAM). 2006. Berlin. Germany.

[21] Яновская Т.Б. Проблемы сейсмотомографии // Проблемы геотомографии. М.: Наука, 1997. С. 86-98.

[22] Bleistein N. Mathematical methods for wave phenomena. Academic Press, 1984. p. 341.

[23] Hung, S., Dahlen, F. & Nolet, G. Wavefront healing: a banana-doughnut perspective. Geophys. J. Int. 2001. vol. 146. pp. 289–312.

[24] Malcolm A.E., Trampert J., Tomographic errors from wave front healing: more than just a fast bias. Geophys. J. Int. 2011. Vol. 185 (1). pp. 385–402.

[25] Starovoytov A.V., Romanova A.M., Kalashnikov A.Yu. GPR study of depressed areas in the upper cross-section. EAGE Near Surface. 2011. Manchester, UK.

[26] Tweeton, D.R., Jackson M.J. and K.S. Roessler. BOMCRATR – A Curved Ray Tomographic Computer Program for Geophysical Applications. 1992. USBM RI 9411. 39.

[27] Lytle R.J, Dines K.A., Laine E.F., and Lager D.L. Electromagnetic Cross-Borehole Survey of a Site Proposed for an Urban Transit Station.1978. UCRL-52484, Lawrence Livermore Laboratory. University of California. 19.

[28] Peterson J. E., Paulson B. N. P., and McEvilly T. V. Applications of Algebraic Reconstruction Techniques to Crosshole Seismic Data. Geophysics. 1985. Vol. 50. pp. 1566-1580.

[29] Lehmann B. Seismic Traveltime Tomography for Engineering and Exploration Applications. 2007. EAGE Publications bv, DB Houton, the Netherlands. pp. 28-32.

[30] Um, J. and C. Thurber. A Fast Algorithm for Two-Point Seismic Ray Tracing. Bulletin of Seismological Society of America. 1987. Vol. 77. pp. 972-986.

[31] Ernst J., Green A., Maurer H., and Holliger K. Application of a new 2D time-domain full-waveform inversion scheme to crosshole radar data. GEOPHYSICS, September-October 2007, Vol. 72. No. 5 : pp. J53-J64

[32] Watson. F. Towards 3D full-wave inversion for GPR. 2016 IEEE Radar Conference (RadarConf). 1-6.

Sudakova M.S., Kalashnikov A.U., Terentieva E.B. GPR tomography as applied to delineation of voids. Construction of Unique Buildings and Structures. 2017. 9(60). Pp. 7-21.

Судакова М.С., Калашников А.Ю., Терентьева Е.Б. Георадарная томография применительно к выявлению пустот, Строительство уникальных зданий и сооружений, 2017, №9 (60). С. 7-21.